Nonlocal photopolymerization kinetics including multiple termination mechanisms and dark reactions. Part II. Experimental validation

Michael R. Gleeson,[1,]* Shui Liu,[1] Robert R. McLeod,[2] and John T. Sheridan[1]

[1]*UCD School of Electrical, Electronic and Mechanical Engineering, UCD Optoelectronic Research Centre, The SFI-Strategic Research Cluster in Solar Energy Conversion, College of Engineering, Mathematical and Physical Sciences, University College Dublin, Belfield, Dublin 4, Ireland*
[2]*Department of Electrical and Computer Engineering, University of Colorado, Campus Box 80309-0425, Boulder, Colorado, USA*
*Corresponding author: michael.gleeson@ucd.ie

In the first of this series of papers [J. Opt. Soc. Am. B **26**, 1736 (2009)], a new kinetic model, which includes most of the major photochemical and nonlocal photopolymerization driven diffusion effects, was proposed. Predictions made using the model were presented, and the numerical convergence of these simulations were examined when retaining higher-concentration harmonics. The validity and generality of the model is examined by applying it to fit experimental data for two different types of photopolymer material appearing in the literature. The first of these photopolymer materials involves an acrylamide monomer in a polyvinylalcohol matrix. The second is a more complex photopolymer in an epoxy resin matrix. Using the new model, key material parameters are extracted by numerically fitting experimentally obtained diffraction efficiency growth curves. The growth curves used include data captured both during exposure and post-exposure, allowing examination and analysis of "dark reactions." © 2009 Optical Society of America

OCIS codes: 090.7330, 090.2900, 050.1940, 160.5335, 160.5470, 300.1030.

1. INTRODUCTION

In Part I [1], a brief review was presented of the photochemical processes involved during holographic grating formation, highlighting some of the assumptions previously made. A general set of governing equations was then derived, which includes the effects of (i) non-steady-state kinetics, (ii) spatially and temporally nonlocal polymer chain growth, (iii) time-varying photon absorption, (iv) diffusion-controlled viscosity effects, (v) multiple termination mechanisms, and (vi) inhibition. From this set of general equations a truncated set of first-order coupled differential equations was generated, and by applying suitable initial conditions, these differential equations were solved numerically. In this way, simulations of the evolution during exposure and post-exposure of the monomer and polymer concentrations were predicted for material parameter values. The temporal evolution of the grating refractive index modulation was then calculated using volume fraction analysis and the Lorentz–Lorenz relation. The numerical convergence of the predictions of the model was then tested, with the retention of 4, 8, and 12 concentration harmonics [1].

In this paper, the validity and generality of this kinetic model [1], is examined by applying it to fit diffraction efficiency measurement data for two different types of photopolymer material previously discussed in the literature. The first of these photopolymer materials is an acrylamide (AA) monomer in a polyvinylalcohol (PVA) matrix, [2,3]. The second material under examination is an epoxy resin matrix, [4,5], which is composed of diethylenetriamine (DTA), and 1,4-butanediol diglycidyl ether (BDGE), with an *N*-vinylcarbozole (NVC) and *N*-vinyl-2-pyrrolidinone (NVP) monomer pairing. Using the kinetic model developed in Part I, key material parameters, such as the polymerization rate constant k_{p}, the bimolecular termination constant k_{t}, the primary termination rate constant k_{tp}, the initiation rate constant k_{i}, and the monomer diffusion coefficient D_{m}, are extracted by fitting the experimentally obtained growth curves. The data analyzed includes information about the growth and/or decay of the grating's strength, both during exposure and post-exposure in order to examine the effects of "dark reactions."

This paper is structured as follows: In Section 2 the photopolymer materials under examination are reviewed. The refractive indices of the main components of each of the photopolymer materials are described using the Lorentz–Lorenz relation. Then, using a previously developed model the key parameters, which determine a material's absorptivity are extracted from fits to experimentally obtained transmission curves in order to predict the rate of generation of primary radicals for a given exposure. In Section 3, using the material parameters obtained in Section 2, the model is applied to extract the key kinetic parameters, which determine a photopolymer material's response under holographic recording conditions. Following this, the results are examined. Finally, in Section 4 a brief conclusion is presented.

2. COMPOSITION, VOLUME FRACTION ANALYSIS, AND ABSORPTION

In order to apply the full general photochemical kinetic model accurately to the photopolymer materials under examination, it is necessary to obtain certain parameters, which determine a photopolymer's behavior. These include the basic composition of the photopolymer material, the ratio of the individual concentrations and volumes of these components, and the absorptive capacity of the material at the recording wavelength. In this section, the aforementioned information is obtained using different experimental and theoretical techniques.

A. AA/PVA Based Photopolymer

We start with an examination of the acrylamide/polyvinylalcohol (AA/PVA) photopolymer. The method of preparation of this material has been previously presented [2,3]. The material consists of a monomer, a binder, a crosslinker (bisacrylamide—BA), an electron donor, (triethanolamine—TEA), and for the specific material under examination here, a photosensitive dye sensitive at λ=532 nm (erythrosin B—EB). Table 3 in [6] lists the standard composition of this material, including the mass, density, and volume of each component. The photosensitizer is not listed because of the low concentration relative to the overall material composition.

1. Volume Fraction Analysis

In the same manner previously described in [6,7], the Lorentz–Lorenz relation is applied to perform a volume fraction and refractive index analysis by combining Eqs. (27–29) in [1] and the volume fraction values presented in Table 3 in [6]. In this way the refractive indices of the individual components, i.e., the monomer refractive index, n_m, the background refractive index, n_b, and the overall refractive index of the photopolymer material before photopolymerization, n_{dark}, were determined following measurements using a prism coupler and application of the Lorentz–Lorenz relation. The resulting values are listed in Table 4 of [6].

Throughout the exposure, monomer is polymerized, thus the amount of polymer increases with time. By assuming that the total volume of the material is conserved during exposure, the total volume fraction of the material remains constant, [6–9]. This results in a direct conversion of monomer volume fraction, $\varphi^{(m)}$, to polymer volume fraction $\varphi^{(p)}$. This enables the evolution of the refractive index modulation to be determined using

$$n_1(t) = \frac{(n_{dark}^2+2)^2}{6n_{dark}}\left[\varphi_1^{(m)}(t)\left(\frac{n_m^2-1}{n_m^2+2}-\frac{n_b^2-1}{n_b^2+2}\right)+\varphi_1^{(p)}(t)\right.$$
$$\left.\times\left(\frac{n_p^2-1}{n_p^2+2}-\frac{n_b^2-1}{n_b^2+2}\right)\right]. \qquad (1)$$

$n_1(t)$ is used in Section 3 in order to predict the temporal evolution of the holographic grating strength, both during and post-illumination.

2. Absorption Parameters

An analysis of the kinetics involved in photon absorption has been examined in [5,6,10–12]. As the generation of primary radicals, which is the driving function of the photopolymerization of monomer, see Eq. (2), is dependent on the amount of light absorbed by the photosensitizer, it is necessary to examine the variation of absorption both during and post-exposure. This can be achieved by (a) measuring the amount of light transmitted during exposure corrected for Fresnel and scattering losses and (b) relating it to the incident intensity [5,6,10–12]. As the molar absorption coefficient, ε (cm²/mol), and quantum yield for the removal of photosensitizer, φ (mol/Einstein), are major factors in determining the material's photochemical behavior, it is important to measure and quantify these parameters accurately. By studying the temporal evolution of the medium transmittance, estimates for these key material parameters have been found [5,6,10–12].

The governing equation for the rate of primary radical production, $R_i(x,t)$, can be expressed as

$$R_i(x,t) = R_i(t)[1+V\cos(Kx)] = 2\Phi I_a(t)[1+V\cos(Kx)], \qquad (2)$$

where Φ is the number of primary radicals produced per photon absorbed, the inclusion of the factor of 2 follows the convention that indicates that two primary radicals are produced for every photon absorbed [13], V is the fringe visibility, and $K=2\pi/\Lambda$ is the grating vector magnitude, where Λ is the grating period.

The resulting time varying absorbed intensity, can be expressed using an adaptation of the Beer–Lambert law [1,5,6,10–13]:

$$I_a(t) = \frac{I_0{}'}{d}\left\{\frac{[\exp(\varepsilon dA_0)-1]\exp(-\varepsilon\varphi I_0{}'t)}{1+[\exp(\varepsilon dA_0)-1]\exp(-\varepsilon\varphi I_0{}'t)}\right\}, \qquad (3)$$

where I_0' (Einsteins/cm² s) is the incident intensity, d (cm) is the photopolymer layer thickness, and A_0 (mol/cm³) is the initial photosensitizer concentration.

Applying these results, experimentally based estimations for ε and φ, for exposure intensities, are given in Table 2 in [11] for 2, 4, and 6 mW/cm² exposure intensities in material layers of thickness $d=120$ μm. These parameters were estimated by fitting experimental transmission curves [5,6,10–12]. Inserting the mean values of these parameters into Eqs. (2) and (3), i.e., $\varepsilon=1.390 \times 10^8$ cm²/mol, $\varphi=0.0348$ mol/Einstein and $T_{sf}=0.7375$, the rate of generation of primary radicals per second was determined and is included into the full general kinetic model, which governs the concentration distributions of primary radicals, macroradicals, monomer, inhibitor, and polymer; see Eqs. (10), (12–15), and (25) in [1], which are used in Subsections 3.B and 3.C.

B. Epoxy Resin Photopolymer

The second photopolymer material examined is the epoxy resin based photopolymer, which was presented originally by Trentler *et al.* [4]. There are a number of major differences between this material and the AA/PVA based photopolymer. The first of these is the thermally cured matrix

Table 1. Functions and Amounts of Each of the Individual Components Needed to Prepare the Epoxy Resin Photopolymer Material [4]

	Component	Acronym	Function	Mass (g)
Matrix				
	Butanediol diglycidyl-ether	BDGE	Epoxide	10.000
	Diethylenetriamine	DTA	Amine Hardener	2.192
Writing Monomer				
	N-vinylcarbazole	NVC	Photopolymerize	0.9629
	N-vinyl-2-pyrrolidinone	NVP	Photopolymerize	0.9629
Photoinitiator				
	Irgacure 784		Radical Initiation	0.0614
Inhibitor				
	Tert-butyl hydroperoxide	TBHP	Bleaching Agent	0.0244
Terminator				
	2,6-Di-tert-butyl-4-methylphenol	BHT	Terminate Polymer Chains	0.0068

network, which allows the epoxy resin type photopolymer material to be cast into large thicknesses and to be sealed or cover-plated on both sides. The second major difference is the difference in the relative refractive indices of the writing monomers to the background material. These two differences give rise to major variations in the behavior of both materials, as will be seen in Section 3. However, significantly, the general kinetic model discussed here, which is based upon the fundamental photokinetic reactions within a photopolymer material, has the ability to predict the behaviors of both of these materials.

1. Composition
The epoxy resin material [4] is prepared by mixing photopolymerizable vinyl monomer with a liquid epoxy resin and an amine hardener. The material hardens providing a solid matrix as the epoxy cures at room temperature. The unreacted vinyl monomers are then ready for photopolymerization. One key feature of this material is the separation of the temperature-based polymerization of the epoxy, which forms a solid matrix, and the vinyl photopolymerizations, which allows the optical recording of index structures [4,14]. The separation of these two types of polymerization makes this material capable of recording large index contrasts between the background and photopolymerized regions. The standard epoxy resin material [4] consists of a low-index matrix, comprising diethylenetriamine, (DTA—hardener), 1,4-butanediol diglycidyl ether, (BDGE—epoxide), and a high refractive index photopolymer mixture of *N*-vinylcarbazole (NVC—writing monomer) and *N*-vinyl-2-pyrrolidinone, (NVP—writing monomer). The Irgacure 784 photoinitiator used is sensitive at $\lambda = 532$ nm.

Table 1 shows the amounts of each of the material components necessary to prepare the photopolymer material with a writing system monomer concentration of approximately 15% of the overall material. The function of each of the material components and their acronyms, which are used from this point forward, are also presented in Table 1.

Using the information about the relative amounts and volumes of each component in the material we can now determine their volume fractions, which will enable us to apply the Lorentz–Lorenz relation to extract information about the time evolution of the refractive index modulation of the holographic grating during exposure and postexposure. This can then be used in the full analysis of this material to extract key material parameters using the model; see Subsection 3.D.

2. Volume Fraction Analysis
Using the same methods described in Section 2.A.1 the volume fractions of the main components of the epoxy resin photopolymer material [4] are examined and presented in Table 2 . The Lorentz–Lorenz expression [1,6–9] is then used to relate these volume fractions to the refractive index changes within the material. These results are presented in Table 3 .

It is assumed that the components presented in Table 2 are the main contributors in terms of volume fractions and refractive indices, (see Table 1). Once again it is assumed that the overall volume of the material is conserved during photopolymerization. Table 3 presents the refractive indices of these main components and the resulting amalgamation of the two writing monomers, NVC and NVP, and the background components, BDGE and DTA. The average refractive index of the material before

Table 2. Volume Fractions of the Main Components in the Epoxy Resin Photopolymer Material [4]

Component	Mass (g)	Density (g/cm^3)	Volume (cm^3)	Volume Fraction
BDGE	10.000	1.100	9.090	0.6864
DTA	2.192	0.955	2.295	0.1750
NVC	0.9629	1.200	0.8024	0.0612
NVP	0.9629	1.040	0.926	0.0706

Table 3. Refractive Index Values for the Main Components of the Epoxy Resin Photopolymer Material Measured and Calculated at $\lambda = 633$ nm

	Component	Refractive Index
n_{NVC}	NVC	1.6800 [4]
n_{NVP}	NVP	1.5112 [4]
n_{BDGE}	BDGE	1.4530 [4]
n_{DTA}	DTA	1.4826 [4]
n_{m}	NVC+NVP	1.5848
n_{b}	BDGE+DTA	1.4590
n_{dark}	NVC+NVP+BDGE+DTA	1.4716

illumination, n_{dark}, was then calculated using the volume fractions given in Table 2. The value for the refractive index of the polymerized monomer is $n_{\text{p}} = 1.5956$ [4]. $n_1(t)$ is then used in Section 3 to predict the temporal evolution of the holographic grating, both during illumination and post-illumination

3. Absorption
Assuming that the same theoretical model used in Subsection 2.A is valid for the Irgacure 784 photosensitizer (see below), transmission curves were obtained and fit for the epoxy resin photopolymer. The photopolymer layers were cast to a thickness $d = 1$ mm and had an initial Irgacure 784 concentration, $A_0 = 1.48 \times 10^{-5}$ mol/cm³, which is different than that given in [4]. The samples were then normally exposed to a plane wave of wavelength $\lambda = 532$ nm. During exposure the evolution of the transmitted intensity was carefully monitored. This measurement was then repeated several times for each exposure intensity: $I_0' = 3$ and 5 mW/cm². Nonlinear fits were then made to these transmission curves, and the parameter values extracted are presented in Table 4. These parameters are used in the analysis and fits presented in Subsection 3.D.

It is known that Irgacure 784 has a more complex set of photokinetic mechanisms than the erythrosin B photosensitiser used in the AA/PVA photopolymer material. These mechanisms can include the generation of photoproducts, which absorb at the exposing wavelength, and also the production of other transient initiator states [15–17]. However, for the short holographic exposures (≤5 s exposure), which are examined in this paper, it is assumed that the simple theoretical model used in the absorption analysis of the AA/PVA system is sufficiently valid in order to estimate the rate of generation of primary radicals $R_i(x, t)$ in the epoxy resin case.

Table 4. Parameter Values Estimated from Transmittance Curves for a Range of Intensities and Constant Layer Thickness $d = 1$ mm in the Epoxy Resin Photopolymer

Intensity (mW/cm²)	ε (cm²/mol) ($\times 10^5$)	φ (mol/Einstein)	T_{sf}
3	1.123	12.13	0.8184
5	1.068	18.38	0.8112

3. GENERAL KINETIC MODEL AND PARAMETER EXTRACTION

In this section a very brief review of the general kinetic model [1] is presented. It is then applied to a continuous exposure growth curve recorded in the AA/PVA system in order to show the functionality of the model for long exposures. Following this, growth curves are presented for both types of photopolymer material for short holographic exposures, with particular attention being paid to the post-exposure effects or dark reactions in both photopolymers. This data is then numerically fit using the model, and key material parameters are estimated and presented.

A. General Kinetic Model
Applying the model presented involves the solutions of the equations, which govern the concentration distributions of primary radicals, macroradicals, monomer, inhibitor, and polymer; see Eqs. (10), (12)–(15), and (25) in [1]. These solutions are then used to generate the time varying monomer and polymer volume fractions necessary for use in Eq. (1). The kinetic rate constants are assumed to be constant as are D_m and D_z, the monomer and inhibitor diffusion rates, respectively.

Since only relatively short exposures are examined, and due to the presence of slight variations in experimental reproducibility, the 4-harmonic kinetic model presented in Part I [1] is used to fit the experimental data. Therefore, the amplitudes of the harmonics of order greater than 3, in the Fourier Series representing the concentrations of the material components, are assumed to be negligible. The result is a set of coupled differential equations, which are solved numerically under the initial conditions, provided in Eq. (19) in [1].

B. Continuous Holographic Exposure (AA/PVA)
An unslanted-transmission-type holographic grating was recorded in the AA/PVA based photopolymer using an exposing intensity of 2 mW/cm² at a spatial frequency of 1000 lines/mm. The growth of the grating was monitored using a probe wavelength , and the resulting first-order diffracted intensity was measured. This data was processed to extract the grating refractive index modulations using Kogelnik's Coupled Wave Theory, [18]. Then, using a least squares algorithm in which the mean square error (MSE) between the prediction and the experimental data was iteratively minimized, the best fit, as a function of the unknown material parameters was obtained. These unknown parameters were restricted to sensible search ranges similar to values in the literature [13,19] (see search range values given in Table 5).

Experimental growth curve data (dots) and the resulting numerical fit, generated using the 4-harmonic kinetic model, can be seen in Fig. 1. As can be seen, the fit is in good general agreement with the experimental data. The parameter values extracted from this fit are as follows: $\sqrt{\sigma'} = 56$ nm, (i.e., $S_1 = 0.94$); $k_{\text{p}} = 3.1 \times 10^6$ cm³ mol⁻¹ s⁻¹; $k_{\text{t}} = 3.5 \times 10^8$ cm³ mol⁻¹ s⁻¹; $k_{\text{tp}} = 3.3 \times 10^{11}$ cm³ mol⁻¹ s⁻¹; $k_{\text{i}} = 4.5 \times 10^7$ cm³ mol⁻¹ s⁻¹; $D_{\text{m}} = 2.8 \times 10^{-11}$ cm² s⁻¹; $k_{\text{z},0} = 5 \times 10^8$ cm³ mol⁻¹ s⁻¹; $D_{\text{z}} = 5 \times 10^{-7}$ cm² s⁻¹; and $n_{\text{p}} = 1.5182$. The mean squared error fit value achieved was

Table 5. Parameter Estimations for Fits to Experimentally Obtained Short Exposure Growth Curves in the AA/PVA Based Photopolymer

t_{exp} (s)	k_p cm^3/mols ($\times 10^6$)	k_t cm^3/mols ($\times 10^8$)	k_{tp} cm^3/mols ($\times 10^{11}$)	k_i cm^3/mols ($\times 10^7$)	D_m cm^2/s ($\times 10^{-11}$)	MSE ($\times 10^{-13}$)
1	2.65	3.5	2.0	4.5	9.0	9.18
2	1.80	1.7	2.0	4.5	4.0	6.91
5	1.70	1.6	2.0	4.4	2.0	11.07
Search Range	0.5–3.5	0.5–4.5	1.0–3.0	3.5–5.5	1.0–12.0	—

$MSE = 4.1 \times 10^{-10}$. As mentioned in Subsection 2.A.2, the absorption parameters used are the mean values presented in Table 2 in [11].

C. Short Exposures and Dark Reactions (AA/PVA)

In previous work [13,20–23] it was assumed that the rate of polymerization responded instantaneously to changes in light intensity, i.e., that there was no temporal response. This assumption results in an instantaneous end to polymerization when the exposure is stopped. However, it has been widely noted that under certain conditions a post-exposure grating amplification can be observed. This effect is caused by a combination of diffusion (material transport) and continued polymer chain growth post-exposure. This process is referred to as dark reactions or post-exposure growth [7,24–27]. These effects are more easily observed in the case of short exposures and, therefore, have a significant effect on applications where short exposure times are used, such as optical data storage [28,29].

Attempts have been made to account for these post-exposure effects in a phenomenological way [7,26,27]. One such method involved the inclusion of a temporal nonlocality into the governing 1-D nonlocal photopolymerization driven diffusion (NPDD) partial differential equation, [7,22,23]:
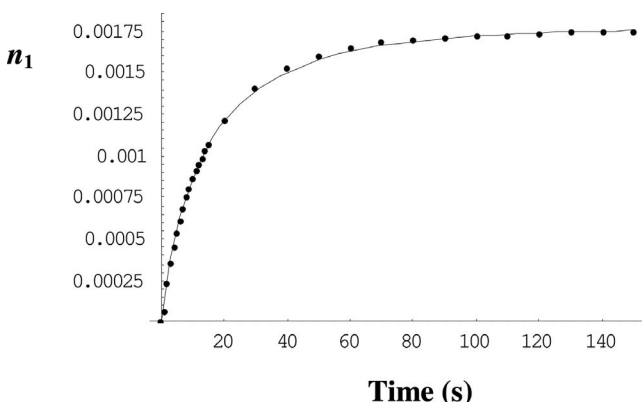

Fig. 1.   Fit (solid line) to an experimentally obtained growth curve (dots) in the AA/PVA based photopolymer material with a continuous exposure of intensity 2 mW/cm^2, using the 4-harmonic model.

$$\frac{du(x,t)}{dt} = \frac{d}{dx}\left[D_m(x,t)\frac{du(x,t)}{dx} \right]$$

$$- \int_{-\infty}^{\infty} \int_0^t G(x,x';t,t')F(x',t')$$

$$\times [u(x',t')]^\beta dt' dx', \qquad (4)$$

where $F(x,t)$ is the polymerization rate and the factor β was introduced to specify the dominant chain termination mechanism, either bimolecular ($\beta=1$) or primary ($\beta=2$) [7,30]. The spatial and temporal nonlocal response function $G(x,x',t,t')$ [7,22,23] represents the effect of polymer chain initiation at location x' and time t' on the amount of monomer polymerized (removed) at location x and time t.

It was assumed [7,22] that the nonlocal response function could be broken up into the product of a spatial and a temporal response, $G(x,x',t,t')=G(x,x')T(t,t')$. The purely temporal part of the response function $T(t,t')$, taking account of the removal of monomer due to past initiations, over the time interval $0 \le t' < t$. The temporal response function proposed was

$$T(t-t') = \frac{1}{\tau_n} \exp\left[\frac{(t-t')}{\tau_n} \right], \qquad (5)$$

where the time constant τ_n determined the extent of the nonlocal temporal response. As τ_n gets smaller the response becomes more localized and $T(t-t')$ approaches a delta function. In this limit the material response function reduces to a purely spatial response equivalent to that given in Eq. (15) in Part I [1].

Using the above analysis, simulations have been generated showing post-illumination effects in AA/PVA photopolymer material. Figure 3 in [7] shows a set of simulations for the refractive index modulation of an unslanted-transmission-type holographic grating. As can be observed in this figure, there is a rapid post-illumination increase in grating strength caused by continuing polymerization of the polymer chains. Following this initial increase, there is a decrease in grating strength, accounted for by the diffusion of monomer (which has a lower refractive index than the background material, $n_m < n_b$ in AA/PVA) into the polymerized regions (exposed areas of high refractive index). This diffusion gives rise to a reduction in the refractive index modulation and therefore a decrease in grating strength.

In the case of the kinetic model presented here, there is no necessity to impose a nonlocal temporal response function as was done in [7]. During short exposures in a monomer-rich environment, the time varying production of primary radicals by photon absorption react with abundant monomer molecules to create macroradicals. These macroradicals, which initiate polymerization, are still present in the material post-exposure. As a result they will continue to react with the monomer present giving rise to further polymerization. This process will continue until all macroradicals are exhausted by one of the termination reactions.

The general kinetic model also accounts for the decrease in grating strength, which occurs when monomer diffusion becomes the dominant post-exposure mechanism (as seen in Fig. 3 in [7]). Once again the post-exposure monomer diffusion results in two simultaneously occurring effects, which cause a drop in the refractive index modulation. First, diffusion of monomer out of the dark regions increases the refractive index of that region ($n_m < n_b$). Second, diffusion of monomer into the exposed bright regions reduces the refractive index of that region ($n_m < n_p$). These two combined effects contribute to an overall reduction in the refractive index modulation.

Figure 2 shows growth curves of refractive index modulation for three different short exposure times: 1 s, 2 s, and 5 s (dots), and the theoretical fit to the experimental data (solid lines), using the 4-harmonic general kinetic model. All gratings were recorded using an incident intensity of 2 mW/cm^2. A 633 nm HeNe laser was again used to monitor the evolution of the grating diffraction efficiencies both during and post-exposure. There is good general agreement between the experimental data and the theoretical fits in Fig. 2. We also note the presence of a dead band region, determined to be of duration 0.2 s, at the start of the growth curves. This appears to be due to inhibition caused by initially dissolved oxygen, which suppresses the photopolymerization process and hence stops grating formation [1,3,6,13].

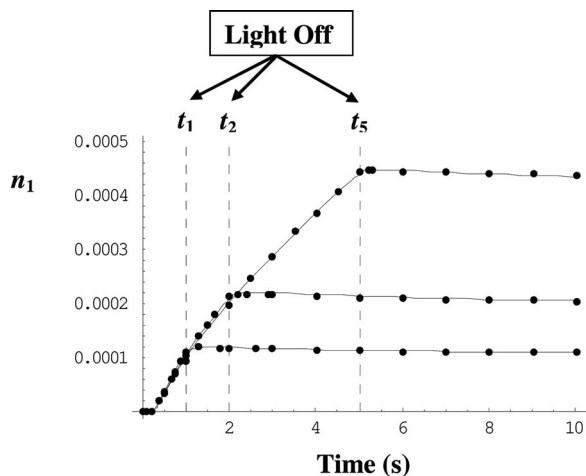Using a least squares algorithm, as before in Fig. 1, best fits were obtained to the data in Fig. 2 as a function of the unknown material parameters, k_p, k_t, k_{tp}, and D_m, using sensible search ranges [13,19]. The values of the inhibition rate and oxygen diffusion were assumed to be constant, $k_{z,0} = 5 \times 10^8$ cm^3 mol^{-1} s^{-1}, $D_z = 5 \times 10^{-7}$ cm^2 s^{-1}. The resulting estimated parameter values are given in Table 5 along with the MSE of each fit. The absorption parameters used were again the mean values from Table II in Ref. [11] for a material layer thickness of 120 μm.

As is evident from the fits presented in Fig. 2 and the MSE values in Table 5, the model predictions very closely fit the experimental data. As stated in Subsection 3.A, the effect of time varying viscosity changes are assumed to be negligible, thus the kinetic parameter values used in the model were treated as constants. However, in the experimental data presented in Fig. 2, we would expect that, with increasing exposure time, there would be an increase in the material's viscosity due to polymerization of the monomer. This increase in viscosity would cause a decrease in the estimated effective kinetic parameters. As the kinetic parameters in the model were treated as constants, the values obtained from the fits would be averages of the kinetic constant over the exposure period. We note that the average kinetic parameter values presented in Table 5 tend to follow the trend expected, i.e., decreasing with increased exposure.

D. Short Exposures and Dark Reactions (Epoxy Resin Photopolymer)

We examine the post-exposure effects, dark reactions, which have been observed in the epoxy resin photopolymer material presented in Subsection 2.B. Combining the volume fraction analysis and the results of the estimates of the absorption parameters, the 4-harmonic kinetic model was fit to reasonably reproducible ($\pm 3\%$) short exposure experimental results, and the kinetic parameters were extracted.

Using the same experimental setup as was used for the previous short-exposure experiments, unslanted holographic gratings were recorded at 1000 lines/mm with an exposure irradiance of 2 mW/cm^2 and wavelength of $\lambda = 532$ nm. The time varying diffraction efficiency $\eta(t)$ was again monitored using a probe wavelength $\lambda = 633$ nm. The diffraction efficiency was appropriately Fresnel corrected and converted into refractive index modulations[18].

In the analysis the initial monomer concentration was calculated to be $U_0 = 9.93 \times 10^{-3}$ mol/cm^3. The initial inhibitor concentration is assumed to be solely due to the included inhibitor TBHP (see Table 1). The concentration of oxygen within the material is therefore assumed to be negligible when compared to the concentration of TBHP, i.e., $Z_0 = 9.58 \times 10^{-6}$ mol/cm^3.

Theoretical best fits were then made to the experimental data and the unknown parameter values extracted and presented in Table 6. Figure 3(a) shows the experimental data (dots) and theoretical fit (dashed curve) for a 5 s holographic exposure and the following 75 s post-exposure. As can be seen, there are significant post-exposure effects, i.e., increases in refractive index modulation. These effects are a result of (i) continued polymerization caused by the large concentration of macroradicals present in the material continuing to react

Fig. 2. Short exposure growth curves of $t_1 = 1$ s, $t_2 = 2$ s, and $t_5 = 5$ s, showing post-exposure effects (dark reactions) in the AA/PVA based photopolymer.

**Table 6. Extracted Parameters from Fits to Short Holographic Exposures in the Epoxy Resin
Photopolymer Material**

Fit (s)	k_p cm^3/mols ($\times 10^7$)	k_t cm^3/mols ($\times 10^9$)	k_{tp} cm^3/mols ($\times 10^{10}$)	k_i cm^3/mols ($\times 10^6$)	D_m cm^2/s ($\times 10^{-11}$)	MSE ($\times 10^{-13}$)
5	1.26	2.6	3.0	8.0	3.5	0.595
80	2.41	2.5	1.0	8.0	2.0	1.848

with monomer-forming polymer and, therefore, increasing the refractive index modulation, and (ii) monomer diffusion from the dark unexposed regions, which as in the AA/PVA photopolymer case has two simultaneous effects. The large contrast between the refractive index of the monomer and background material in the epoxy resin based photopolymer, i.e., $n_m > n_b$ (see Table 3) results in a substantial drop in the refractive index in the dark regions when the monomer diffuses out to the depleted bright regions. Simultaneously, monomer diffusion leads to an increase in the refractive index of the exposed region it diffuses into, further increasing the refractive index modulation. This can be observed in Fig. 3(a). Thus the main difference between the behaviors of the two photopolymer systems being examined post exposure is the relative refractive index differences between the monomer and the background materials.
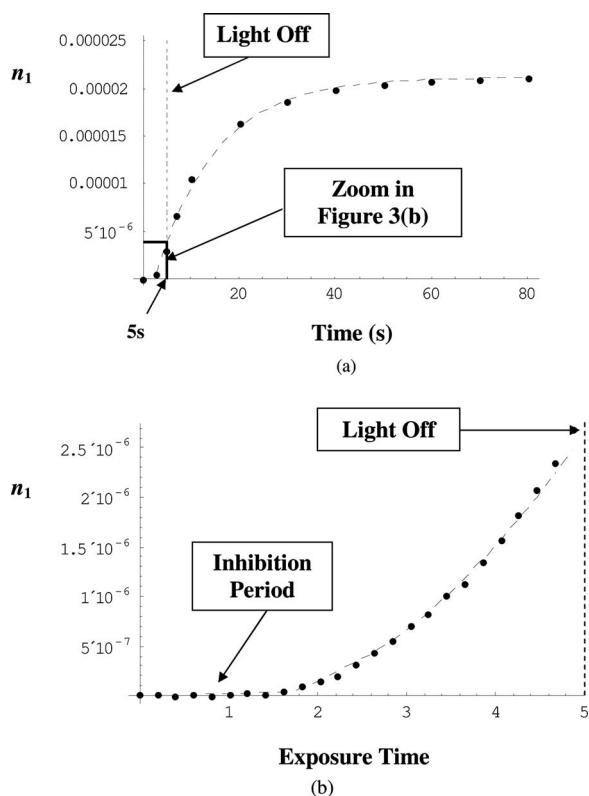

Fig. 3. (a) Experimental data (dots) and theoretical fit (long dashed curve) of the post-exposure dark reactions for a 5 s short exposure with 2 mW/cm^2 in the epoxy resin photopolymer material. (b) Zoomed-in window of the experimental data (dots) and theoretical fit (dashed curve) presented in (a) for a 5 s short exposure with 2 mW/cm^2 in the epoxy resin photopolymer material.

Figure 3(b) shows the initial 5 s of Fig. 3(a). It can be seen that there is good general agreement between experimental data and the theoretical predictions. One thing of note is the dead-band period, which is associated with the induction (initiation) and inhibition period, which lasts for approximately 1.5 s. As mentioned earlier, in this epoxy resin material analysis the TBHP inhibitor is assumed to be the dominant inhibitor present within the material and, as can be observed from the experimental data, it causes a substantial dead-band.

Fits were carried out just for the 5 s subsection, i.e., for the subsection 5 s shown in Fig. 3(b), and also for the full growth curve including the full dark reaction region, i.e., 80 s, as presented in Fig. 3(b). In both cases the nonlocal material response length was chosen to be $\sqrt{\sigma'}=56$ nm (i.e., $S_1=0.94$), and the inhibition rate constant was assumed to be $k_z=5\times 10^8$ cm^3/mols. The best-fit parameter values obtained from both these fits are presented in Table 6. It can be seen that there is reasonable agreement between the kinetic parameters extracted from the two fits. One plausible reason for the variation seen between the extracted parameter values could be the neglect of time varying viscosity effects. However, the low MSE values obtained suggest that the theoretical model satisfactorily predicts the behavior of this epoxy resin photopolymer material well, and thus that the model presented is physically valid for at least two significantly different types of photopolymer materials.

The model was also used to fit the experimental data presented in Fig. 4 for short holographic exposures of 3 s, 6 s, and 10 s. Once again a large amount of post-exposure growth in the refractive index modulation can be observed. The parameters extracted from these fits are presented in Table 7. The nonlocal material response length was again chosen to be $\sqrt{\sigma'}=56$ nm (i.e., $S_1=0.94$), and
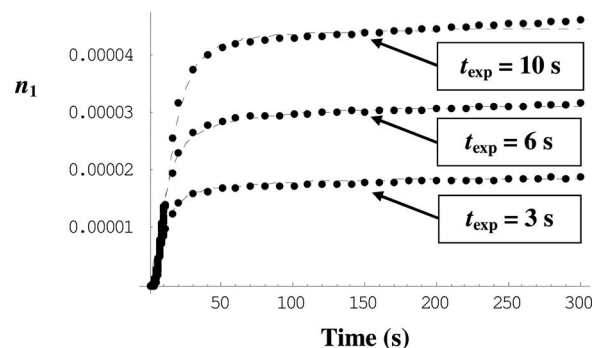

Fig. 4. Experimental data (dots) and theoretical fit (long dashed curve) of the post-exposure dark reactions for short exposures of $t_{exp}=3$ s, $t_{exp}=6$ s, and $t_{exp}=10$ s in the epoxy resin photopolymer material with an exposure intensity of 2 mW/cm^2.

Table 7. Extracted Parameters from Fits to Short Holographic Exposures in the Epoxy Resin Photopolymer Material for an Exposure Intensity of 2 mW/cm²

t_{exp} (s)	k_p cm³/mols ($\times 10^7$)	k_t cm³/mols ($\times 10^9$)	k_{tp} cm³/mols ($\times 10^{10}$)	k_i cm³/mols ($\times 10^6$)	D_m cm²/s ($\times 10^{-11}$)	MSE ($\times 10^{-13}$)
3	2.80	1.61	3.3	8.1	2.5	1.90
6	2.43	2.6	3.0	8.0	3.0	10.09
10	2.30	1.39	3.3	8.0	3.0	18.01

the inhibition rate constant assumed to be $k_z = 5 \times 10^8$ cm³/mols. The MSE values are again relatively good. However, as can be seen from Fig. 4, there is a slight deviation between the fits and the experimental data for large post-exposure times. Again a plausible reason for this variation could be due to the neglect of time varying viscosity effects.

4. CONCLUSIONS

In this paper, the generality of the previously developed photokinetic model [1] of the photochemical processes involved during holographic grating formation has been experimentally tested. This was achieved by numerically fitting experimentally obtained growth curves for two types of photopolymer material, which differ in (a) the type of photosensitizer, (b) the material layer thickness, (c) the type of matrix network used, and (d) the ratio of the refractive index of the writing monomer to the refractive index of the background material. The first of these photopolymer materials examined was an AA/PVA based photopolymer [2,3], and the second was an epoxy resin based photopolymer [4].

In order to experimentally validate the proposed model, material parameters for each of the compositions under examination were obtained. These included the molar absorption coefficient, ε, and the quantum efficiency for the removal of the photosensitizer, φ. These were acquired by numerically fitting experimental transmission curves for each of the material compositions using the theoretical model presented in [5,6,10–12]. In this way a reasonable approximation to the rate of generation of primary radicals for a given exposure could be determined. Other material parameters necessary included the volume fractions and refractive indices of the individual components of each of the photopolymers. From this analysis a better approximation to the time varying refractive index modulation was obtained. Both sets of analysis are described in Section 2.

In Section 3, using the parameters obtained in Section 2, the model was then applied to fit experimental data for short holographic exposures including inhibition and post-exposure effects (dark reactions) in both types of photopolymer. Physical parameter values were thus extracted from experimental short exposure data. The fits found are in good agreement with the experimental data, indicated by the low MSE values achieved. Furthermore, the values obtained for the extracted parameter values all lay within the expected ranges as indicated in the literature. Comparing the parameter values extracted for the same materials, and noting that these have been found

for average data sets and with very low MSE values, it should be clear that the parameter values estimated are robust and, under the assumptions made, are very close to the true effective values. What we have also found is that the MSE values increase very rapidly if the parameter values are randomly perturbed.

Certain assumptions were, however, made in order to reduce the complexity of the fitting procedure. These include assuming negligible viscosity changes within the material during exposures, which results in the estimation of constant time-independent diffusion and kinetic parameters. Currently, work is being carried out to (a) more accurately determine the change in the rate of monomer diffusion D_m with exposure, (b) to find the glass transition temperatures T_g, (c) the expansion coefficients α_m, α_p, and (d) the fractional free volumes of the material f^v [1,19]. These values will enable a more accurate determination of the temporal variation of the photochemical kinetics in the materials and should result in an improvement in fit quality. Furthermore, a more physically realistic model of the absorption mechanisms of the Irgacure 784 photosensitizer needs to be used in conjunction with the general kinetic model in order to more accurately predict the primary radical initiation rate. It should also be noted that material shrinkage and swelling effects can occur during and post exposure, [31,32]. These effects can be modeled by introducing holes into the volume fraction analysis [31,33]. The accurate modeling of such effects will involve multicomponent kinetics, which also have not been included here [25,31,33]. However, even with the exclusion of all of these physical effects, which have yet to be implemented into the general NPDD model, the quality of the fits by way of MSE are considerably better (two orders of magnitude) than the fits achieved with previous models [3,6,7,22,23,31].

REFERENCES

1. M. R. Gleeson and J. T. Sheridan, "Nonlocal photopolymerization kinetics including multiple termination mechanisms and dark reactions. Part I. General model," J. Opt. Soc. Am. B **26**, 1736–1745 (2009).

2. J. R. Lawrence, F. T. O'Neill, and J. T. Sheridan, "Photopolymer holographic recording material," Optik (Stuttgart) **112**, 449–463 (2001).
3. M. R. Gleeson, J. V. Kelly, and J. T. Sheridan, "Modelling the photochemical effects present during holographic grating formation in photopolymer materials," J. Appl. Phys. **102**, 023108 (2007).
4. T. Trentler, J. Boyd, and V. Colvin, "Epoxy resin photopolymer composites for volume holography," Chem. Mater. **12**, 1431–1438 (2000).
5. M. R. Gleeson, "Analysis of the photochemical kinetics in photopolymers for holographic data storage and hybrid photonic circuits," Ph.D. thesis (University College Dublin, 2008).
6. M. R. Gleeson, D. Sabol, S. Liu, C. E. Close, J. V. Kelly, and J. T. Sheridan, "Improvement of the spatial frequency response of photopolymer materials by modifying polymer chain length," J. Opt. Soc. Am. B **25**, 396–406 (2008).
7. J. V. Kelly, M. R. Gleeson, C. E. Close, F. T. O'Neill, J. T. Sheridan, S. Gallego, and C. Neipp, "Temporal analysis of grating formation in photopolymer using the nonlocal polymerization-driven diffusion model," Opt. Express **13**, 6990–7004 (2005).
8. V. L. Colvin, R. G. Larson, A. L. Harris, and M. L. Schilling, "Quantitative model of volume hologram formation in photopolymers," J. Appl. Phys. **81**, 5913–5923 (1997).
9. I. Aubrecht, M. Miler, and I. Koudela, "Recording of holographic diffraction gratings in photopolymers: Theoretical modelling and real-time monitoring of grating growth," J. Mod. Opt. **45**, 1465–1477 (1998).
10. L. Carretero, S. Blaya, R. Mallavia, R. F. Madrigal, A. Belendez, and A. Fimia, "Theoretical and experimental study of the bleaching of a dye in a film-polymerization process," Appl. Opt. **37**, 4496–4499 (1998).
11. M. R. Gleeson, S. Liu, S. O'Duill, and J. T. Sheridan, "Examination of the photoinitiation processes in photopolymer materials," J. Appl. Phys. **104**, 064917 (2008).
12. S. Liu, M. R. Gleeson, and J. T. Sheridan, "Analysis of the photoabsorptive behavior of two different photosensitizers in a photopolymer material," J. Opt. Soc. Am. B **26**, 528–536 (2009).
13. G. Odian, *Principles of Polymerization* (Wiley, 1991).
14. A. C. Sullivan, M. W. Grabowski, and R. R. McLeod, "Three-dimensional direct-write lithography into photopolymer," Appl. Opt. **46**, 295–301 (2007).
15. J. Jakubiak and J. F. Rabek, "Photoinitiators for visible light polymerisation," Polimery **44**, 447–461 (1999).
16. S. H. Lin, Y.-N. Hsiao, and K. Y. Hsu, "Preparation and characterization of Irgacure 784 doped photopolymers for holographic data storage at 532 nm," J. Opt. A, Pure Appl. Opt. **11**, 024012 (2009).
17. D. Sabol, M. R. Gleeson, S. Liu, and J. T. Sheridan, "Photokinetic study of Irgacure 784," Proc. SPIE **7358**, 735804 (2009).
18. H. Kogelnik, "Coupled wave theory for thick hologram gratings," Bell Syst. Tech. J. **48**, 2909–2945 (1969).

19. M. D. Goodner, H. R. Lee, and C. N. Bowman, "Method for determining the kinetic parameters in diffusion-controlled free-radical homo-polymerizations," Ind. Eng. Chem. Res. **36**, 1247–1252 (1997).
20. G. H. Zhao and P. Mouroulis, "Diffusion-model of hologram formation in dry photopolymer materials," J. Mod. Opt. **41**, 1929–1939 (1994).
21. J. H. Kwon, H. C. Hwang, and K. C. Woo, "Analysis of temporal behavior of beams diffracted by volume gratings formed in photopolymers," J. Opt. Soc. Am. B **16**, 1651–1657 (1999).
22. J. T. Sheridan and J. R. Lawrence, "Nonlocal-response diffusion model of holographic recording in photopolymer," J. Opt. Soc. Am. A **17**, 1108–1114 (2000).
23. J. R. Lawrence, F. T. O'Neill, and J. T. Sheridan, "Adjusted intensity nonlocal diffusion model of photopolymer grating formation," J. Opt. Soc. Am. B **19**, 621–629 (2002).
24. C. Decker, B. Elzaouk, and D. Decker, "Kinetic study of ultrafast photopolymerizations reactions," J. Macromol. Sci., Pure Appl. Chem. **A33**, 173–190 (1996).
25. H. M. Karpov, V. V. Obukhovsky, and T. N. Smirnova, "Generalized model of holographic recording in photopolymer materials," Semicond. Phys., Quantum Electron. Optoelectron. **2**, 66–70 (1999).
26. M. Toishi, T. Tanaka, K. Watanabe, and K. Betsuyaku, "Analysis of photopolymer media of holographic data storage using non-local polymerization driven diffusion model," Japanese J. Appl. Phys. Part 1 **46**, 3438–3447 (2007).
27. M. Toishi, T. Takeda, K. Tanaka, T. Tanaka, A. Fukumoto, and K. Watanabe, "Two-dimensional simulation of holographic data storage medium for multiplexed recording," Opt. Express **16**, 2829–2839 (2008).
28. R. R. McLeod, A. J. Daiber, M. E. McDonald, T. L. Robertson, T. Slagle, S. L. Sochava, and L. Hesselink, "Microholographic multiplayer optical disk data storage," Appl. Opt. **44**, 3197–3207 (2005).
29. InPhase Technologies, "www.inphase-technologies.com" Tapestry Media, (2007).
30. S. Blaya, L. Carretero, R. F. Madrigal, M. Ulibarrena, P. Acebal, and A. Fimia, "Photopolymerization model for holographic gratings formation in photopolymers," Appl. Phys. B **77**, 639–662 (2003).
31. J. V. Kelly, M. R. Gleeson, C. E. Close, F. T. O'Neill, J. T. Sheridan, S. Gallego, and C. Neipp, "Temporal response and first order volume changes during grating formation in photopolymers," J. Appl. Phys. **99**, 113105 (2006).
32. F. T. O'Neill, A. J. Carr, S. M. Daniels, M. R. Gleeson, J. V. Kelly, J. R. Lawrence, and J. T. Sheridan, "Refractive elements produced in photopolymer layers," J. Mater. Sci. **40**, 4129–4132 (2005).
33. R. L. Sutherland, V. P. Tondiglia, L. V. Natarajan, and T. J. Bunning, "Phenomenological model of anisotropic volume hologram formation in liquid-crystal-photopolymer mixtures," J. Appl. Phys. **96**, 951–965 (2004).